Reaktor

p-ISSN 0852 – 0798
e-ISSN 2407 – 5973

Website: http://ejournal.undip.ac.id/index.php/reaktor/

Reaktor, Vol. 25 No. 1, April Year 2025, pp. 36-46

Adsorption Photocatalytic Removal of Rhodamine B using Dodecyl Dimethyl Betaine (BS12) Intercalated Silver Tetratungstate-Bentonite composites: Effect of Ag and Surfactant Loading, pH, and its Subsequent Economic Feasibility

Siswo Sumardiono[1,*)], Fajar Kasih Setiawan[1)], Bakti Jos[1)], and Heri Cahyono[1)]

[1)]Department of Chemical Engineering, Faculty of Engineering, Universitas Diponegoro
Semarang 50275, Indonesia

[*)] Corresponding author: siswo.sumardiono@che.undip.ac.id

(Received: 17 July 2025; Accepted: 26 August 2025; Published: 8 September 2025)

Abstract

The potential of silver tetratungstate-doped bentonite intercalated with zwitterionic surfactant for removing Rhodamine B (RhB) was evaluated by comparing three composites, namely, AB (acid-activated bentonite), AB impregnated with $Ag_8W_4O_{16}$ photocatalyst (Ag@AB), and Ag@AB intercalated with dodecyl dimethyl betaine (BS12) *surfactant (Ag@OAB) with respect to their photocatalytic adsorption performance. The AB composite was prepared by treating natural bentonite with hydrochloric acid (HCl). Next, Ag@AB was synthesized by wet impregnation of $Ag_8W_4O_{16}$ onto AB. Lastly, the Ag@OAB was formed by intercalating the BS12 surfactant onto the Ag@AB composite. The morphology of the composite structures was characterized using Scanning Electron Microscopy (SEM). The addition of 4% Ag (w/w) tetratungstate W_4O_{16} and 50% CEC BS12 to AB produced RhB removal percentages of 66% and 59%, respectively, compared to 65% for AB. The maximum removal percentage was achieved at pH 4 for the AB, Ag@AB, and Ag@OAB composites with RhB removal percentages of 67%, 71%, and 44%, respectively. The AB composite showed the highest regenerative ability compared to Ag@AB and Ag@OAB, with AB maintaining RhB removal at 70% after five regeneration cycles, while Ag@AB and Ag@OAB only reached four and three regeneration cycles. The total production cost of AB is fourteen to sixteen times lower than that of Ag@AB and Ag@OAB composites. In summary, the impregnation of the $Ag_8W_4O_{16}$ photocatalyst onto AB, resulting in the Ag@AB composite, increases the RhB removal efficiency compared to pristine AB. In contrast, the intercalation of the BS12 surfactant in Ag@OAB composite led to a decrease in RhB removal efficiency, resulting in the lowest performance among the three composites.*

Keywords: adsorption; photocatalytic; bentonite; dodecyl dimethyl betaine; rhodamine B; silver tetratungstate

How to Cite This Article: Sumardiono, S., Setiawan, F.K., Jos, B., and Cahyono, H., (2025), Adsorption Photocatalitic Removal of Rhodamine B using Dodecyl Dimethyl Betaine (BS12) Intercalated Silver Tetratungstate-Bentonite composites: Effect of Ag and Surfactant Loading, pH and its Subsequent Economic Feasibility, Reaktor, 25 (1), 36 - 46, https://doi.org/10.14710/reaktor. 25. 1. 36 - 46

INTRODUCTION

The global production of synthetic dyes is estimated at approximately 70 million tonnes annually, of which nearly 800,000 tonnes are used in textile dyeing processes within the fashion industry (Islam et al., 2023). Unfortunately, most of these dyes exhibit limited affinity for textile fibers, resulting in half of the dyes remaining unadsorbed during the dyeing process (Markandeya et al., 2022). These excess dyes are subsequently discharged as textile dye wastewater, which poses significant environmental hazards. The release of such effluents into aquatic ecosystems has been shown to severely impact aquatic life, including increased mortality rates in freshwater fish species such as *Cirrhinus mrigala* (Hussain et al., 2021). Additionally, the infiltration of textile dye wastewater into soil systems can inhibit plant growth by disrupting essential nitrogen absorption processes (Chandanshive et al., 2018). The accumulation of these pollutants in surface water poses a significant health risk to humans, including an increased risk of cancer, skin irritation, and internal damage to the digestive and excretory systems (Al-Tohamy et al., 2022).

One of the conventional methods for removing textile dye waste is adsorption using adsorbent composites. Adsorption is economically cost-effective and easy to operate compared to other methods such as coagulation, ozonation, and oxidation (Djebri et al., 2016). However, a limitation of the adsorption method is its reduced effectiveness at maximum adsorption capacity, which is due to the nature of the adsorption mechanism (Rafiq et al., 2021). To overcome this limitation, bentonite—one of the primary adsorbents used for dye removal—was modified by impregnating it with a photocatalyst and intercalating a zwitterionic surfactant onto its surface.

In recent years, the impregnation of photocatalysts and the intercalation of surfactants into clay surfaces have been widely studied in water treatment research. Metal-based photocatalysts, particularly tungstates doped with silver, such as $AgWO_3$ (Aslam et al., 2019), Ag_2WO_4 (Zinatloo-Ajabshir et al., 2020), and $Ag_8W_4O_{16}$ (Wang et al., 2014), have garnered significant attention due to their wide band gaps and high photocatalytic efficiency in dye decolorization. In this study, silver tetratungstate ($Ag_8W_4O_{16}$) was selected as the photocatalyst and further impregnated onto bentonite. $Ag_8W_4O_{16}$ has a band gap energy of approximately 3.15 eV and a broad absorption range in visible light (400–500 nm) (Wang et al., 2014). Another advantage of silver tetratungstate is the simplicity of its synthesis, which involves only mixing the precursors $AgNO_3$ and Na_2WO_4 at ambient temperature (Wang et al., 2011). However, a drawback of using the photocatalyst alone is its susceptibility to aggregation, which reduces its photocatalytic efficiency (Laysandra et al., 2017). To address this issue, the photocatalyst was immobilized within the bentonite structure using a wet impregnation method.

One of the conventional methods for removing textile dye waste is adsorption using adsorbent composites. Adsorption is an economically low-cost and easy-to-operate method compared to other methods, such as coagulation, ozonation, and oxidation. However, one limitation of the adsorption method is its low effectiveness at the saturation point, which is caused by the adsorption mechanism (Rafiq et al., 2021). To overcome this limitation, a major adsorbent for removing dye waste, bentonite, was modified by impregnating a photocatalyst and intercalating a zwitterionic surfactant onto its surface. In recent years, the impregnation of photocatalysts and the intercalation of surfactants into clay surfaces have been studied in water treatment research. Metal-based photocatalysts, such as $AgWO_3$ (Aslam et al., 2019), Ag_2WO_4 (Zinatloo-Ajabshir et al., 2020), and $Ag_8W_4O_{16}$ (Wang et al., 2014), which are doped with tungstate and silver, have garnered attention due to their wide band gap and photocatalytic efficiency for dye decolorization in wastewater. In this study, silver tetratungstate ($Ag_8W_4O_{16}$) was used as photocatalyst, which was further impregnated onto bentonite. $Ag_8W_4O_{16}$ has a band gap energy of approximately 3.15 eV and exhibits broad absorption in the visible light range of 400 –500 nm (Wang et al., 2014). Another advantage of silver tetratungstate is its simplicity of synthesis, which involves only mixing the precursors $AgNO_3$ and Na_2WO_4 at ambient temperature (Wang et al., 2011). However, one drawback of using the photocatalyst alone is its susceptibility to aggregation, which reduces photocatalytic ability (Laysandra et al., 2017). To overcome this problem, the photocatalyst was immobilized in the bentonite structure through the wet impregnation method.

Natural clay, such as bentonite or montmorillonite, is recognized for its large surface area, high adsorption capability, and low cost, and is widely utilized as a dye wastewater adsorbent (Ulhaq et al., 2021). Indonesia has abundant natural montmorillonite deposits, estimated at around 500 million tonnes at more than 29 locations (Ramadhan et al., 2015). Despite the availability of natural resources, Indonesia still imports 20% of its bentonite for industrial purposes (Warsono et al., 2018). Therefore, natural bentonite was used as a photoadsorbent support in this study. However, the impregnation of photocatalyst onto bentonite does not alter its hydrophilic nature, which can make it challenging to remove zwitterionic dyes, such as Rhodamine B (RhB).

Therefore, a zwitterionic dodecyl dimethyl betaine (BS12) surfactant was used in this study (Yang et al., 2020). The intercalation of BS12 in clay has been studied for the adsorption of metal ions and phenolic compounds in aqueous solutions (Li et al., 2023; Ren et al., 2019). In this study, three distinct composites, namely acid-activated bentonite (AB), AB impregnated with $Ag_8W_4O_{16}$ photocatalyst (Ag@AB), and Ag@AB intercalated with *dodecyl*

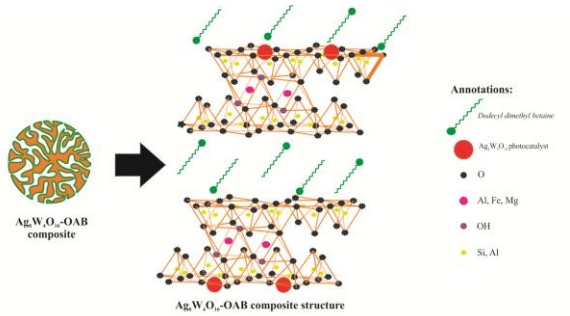

Figure 1. The cross-section structure of Ag@OAB ($Ag_8W_4O_{16}$-OAB) composite

dimethyl betaine (Ag@OAB), which are shown in Fig. 1, were compared in terms of their capabilities in removing RhB dye. The effect of Ag% (w/w) and BS12 surfactant (CEC AB) loading on AB on the removal of RhB was studied. Additionally, the influence of pH on RhB removal efficiency and its impact on changes in the surface charge of the composites were also studied. Furthermore, composite regeneration and its subsequent total fabrication cost were studied in an economic feasibility study.

MATERIALS AND METHODS

Materials

Bentonite was obtained naturally from the Sidoarjo mudflow in East Java, Indonesia, and was used without further purification. Sodium tungstate dihydrate (99% purity), silver nitrate (99% purity), hydrochloric acid (37% w/v), sodium hydroxide (99% purity), trisodium citrate (99% purity), nitric acid (65% w/v), and Rhodamine B (95% purity) were imported from Merck. The amphoteric surfactant, dodecyl dimethylbetaine (BS12), was purchased from Kao Chemical Indonesia under the brand name Amphitol 20B (26% w/v).

Synthesis of Acid-Activated Bentonite (AB)

Acid-activated bentonite (AB) was synthesized via an acid pretreatment method. A total of 10 grams of natural bentonite (particle size -100/+200 mesh) was dispersed in 200 mL of 5 N hydrochloric acid solution. The suspension was stirred continuously at 100 rpm and 80 °C for 1 hour. Following activation, the resulting AB precipitate was filtered and rinsed with deionized water until a neutral pH was achieved. The AB was then dried in an oven at 80 °C for 12 h and subsequently stored in a desiccator for future use.

Synthesis of Ag@AB Composite

The Ag@AB composite was prepared by wet impregnation of $Ag_8W_4O_{16}$ nanoparticles onto AB. Sodium tungstate dihydrate (13.31 g) and silver nitrate (0.32 g) were dissolved in 200 mL of deionized water at room temperature under continuous stirring at 300 rpm for 1 h. The pH of the solution was then adjusted to 10 with 0.01 M sodium hydroxide, and stirring was continued for an additional 30 min. The pH of the solution was adjusted to 10 using 0.01 M sodium hydroxide and stirred for an additional 30 minutes. During this process, the solution color changed from milky white to a yellowish hue. Subsequently, risodium citrate (0.48 g) was added dropwise under constant stirring for 1 h, inducing a color change from yellowish to brownish, indicating the reduction of silver ions and the formation of Ag-tungstate complexes. The solution was then decanted and stored in a sealed, tinfoil-wrapped container for 24 hours to facilitate the formation of $Ag_8W_4O_{16}$ nanoparticles. Next, AB (20 g) was introduced into the nanoparticle solution and stirred at 100 rpm for 1 h at room temperature. The resulting Ag@AB precipitate was filtered, rinsed with deionized water until neutral pH was attained, and dried at 60 °C for 10 h. The final composite was stored in a desiccator.

Synthesis of Ag@OAB Composite

The Ag@OAB composite was synthesized by intercalating the BS12 surfactant into the Ag@AB composite. A BS12 solution was prepared by dissolving 30.2 mL of BS12 surfactant in 200 mL of deionized water. Then, Ag@AB (5 g) was introduced into the solution and stirred at 100 rpm for 3 h at 40 °C. The resulting mixture was stored in a sealed, tinfoil-wrapped container for 24 hours to promote intercalation. The Ag@OAB precipitate was subsequently filtered and rinsed with deionized water until no bubbles were observed in the filtrate, confirming the removal of excess surfactant. The final sample was dried at 80 °C for 10 h and stored in a desiccator for future use.

Photocatalytic Adsorption Experimental Setup

The photocatalytic adsorption performance of AB, Ag@AB, and Ag@OAB composites was evaluated by monitoring the final concentration of RhB at any given time using a UV-Vis spectrophotometer at a wavelength of 546 nm. The experiments utilized a 50×60×100 cm aluminum-lined chamber, equipped with a hotplate and a SINJIA ZW0186 40 W full-spectrum LED lamp (comprising 40 LEDs: 24 red at 730 nm, 8 blue at 495 nm, 2 white full-spectrum, 2 warm white full-spectrum, 2 infrared >730 nm, and 2 ultraviolet <410 nm). All tests were performed in a temperature-controlled, closed environment to prevent external light interference.

Preliminary experiments were conducted to optimize RhB removal by varying Ag loading (% w/w tetratungstate) and BS12 surfactant concentration (% CEC of AB). In each experiment, composite (0.2 g) was added to 100 mL of 50 mg/L RhB solution at pH 6.5. The solution was stirred at 100 rpm under irradiation for 1 hour at ambient temperature. Residual RhB concentration was quantified using a UV–Vis spectrophotometer at 546 nm. The percentage of RhB removal was calculated using Equation (1):

$$\%RhB\ removal = \frac{C_i - C_f}{C_f} \times 100\% \quad \text{.....(1)}$$

where C_i and C_f were the initial and final concentrations of RhB (mg/L). After the optimum Ag loading (% w/w tetratungstate W_4O_{16}) and BS12 surfactant concentrations (%CEC of AB) were found, Ag@AB and AgOAB composites were synthesized.

The influence of pH on the AB, Ag@AB, and Ag@OAB composites was investigated by varying the RhB solution pH from 4 to 1 using 0.01 M NaOH and 0.01 M HCl solutions. The composite (0.2 g) was added to 100 mL of 50 mg/L RhB solution at each varying pH. The solution was stirred at 100 rpm under irradiation for 1 hour at ambient temperature. The final concentration was then determined using a UV-Vis spectrophotometer. The percentage of RhB removal was calculated using Equation (1). The point of zero charge (pHpzc) of each composite was determined using the exact solutions over the same pH range as before. The composite samples (0.2 g) were dispersed in 100 mL of deionized water adjusted to the designated pH. Then, the solutions were stirred for 1 hour and stored in the dark at ambient temperature for 24 hours. After that, the final pH was determined using a pH meter.

Economic feasibility was assessed by comparing the three composites through composite regeneration in repeated cycles and calculating the total fabrication cost incurred during composite production. Regeneration of composites was performed by submerging spent composites in a 0.1 M NaOH solution, then washing them three times until the pH was neutral. Then, the spent composites were dried at 60 °C for 10 hours. 1 gram of the composite was added to 100 mL of a 200 mg/L RhB solution at pH 4. The solution was stirred for 1 hour at ambient temperature. The final concentration was then determined using a UV-Vis spectrophotometer. The regenerative ability of the composites is calculated using Equation (2) given below (Aichour & Zaghouane-Boudiaf, 2020):

$$\%n^{th}\text{ cycle of RhB removal} = \frac{C_i - C_f}{C_i} \times 100\% \quad \text{----------(2)}$$

where C_i and C_f are the initial and final concentrations of RhB, while n^{th} denotes the number of regeneration cycles.

The estimation of total fabrication cost (TFC) is calculated from the total cost of feedstock, including raw materials procurement, production cost, and its additional cost given by Equation (3) below (Cheng et al., 2020):

$$\text{TFC} = \text{raw material cost} + \text{production cost} + \text{additional cost} \quad \text{----------(3)}$$

The production cost is calculated as the total energy cost used during the production of the three composites. The cost of energy in Equation (3) can be calculated using Equation (4) written below (Balakrishnan et al., 2021):

$$\text{Production cost(kWh)} = \frac{\text{Power consumed (W)} \times \text{reaction time(min)} \times \text{power cost } (\frac{\text{IDR}}{\text{kWh}})}{60 \times 1000} \quad \text{----------(4)}$$

Additional costs incurred during production, such as washing, packaging, and material transportation, were not accounted for in this study.

Characterization Method

The characterization of AB, Ag@AB, and Ag@OAB composites was done using SEM (Scanning Electron Microscope). The surface morphology of the three composites was determined using an SEM (Jeol JSM 6510) at 500 and 2000 magnification. The pHpzc values of all three composites were determined using the pH drift method (Saha et al., 2020). The CEC (Cation Exchange Capacity) value of the AB composite was determined using the Brown method (Rihayat et al., 2018), which yielded a value of 66.4 meq/100 g AB.

RESULTS AND DISCUSSION

Scanning Electron Microscopy Analysis

The surface morphology of the AB and Ag@OAB composite presented in Figure 2. The surface of AB is revealed to be porous and rough, as seen in 1000 and 5000 × magnification while the Ag@OAB composite tends to form aggregates with each other. This aggregation suggests the successful intercalation of BS12 surfactant into Ag@AB, leading to the formation of Ag@OAB (Li et al., 2023). The porous and rough surface of AB provides many active sites, which is beneficial for supporting photocatalyst impregnation and facilitating surfactant intercalation onto AB surface (Nan et al., 2025).

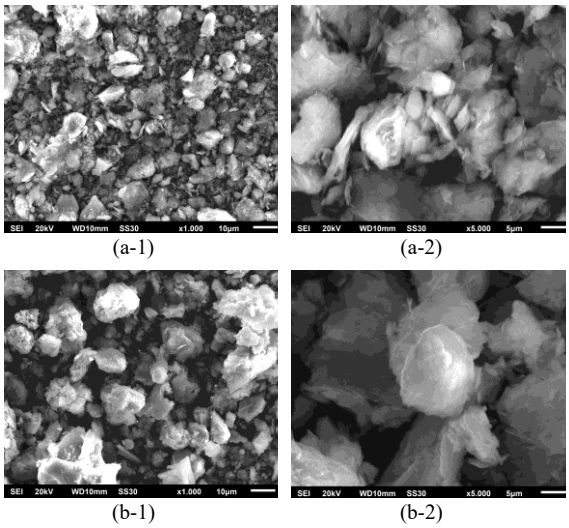

(a-1) (a-2)

(b-1) (b-2)

Figure 2. SEM results of (a) AB and (b) Ag@OAB composite; surface images at (1) ×1000 and (2) ×5000 magnification

While the aggregation and successful intercalation in Ag@OAB facilitate stronger interactions between photocatalyst nanoparticles and the support. This structural feature is directly aligned with the aim of generating a composite with enhanced adsorption capacity and photocatalytic efficiency for RhB removal. This structural feature is directly aligned with the aim of generating a composite with enhanced adsorption capacity and photocatalytic efficiency for RhB removal.

Effect of Ag% (w/w% W_4O_{16}) and BS12 Surfactant (%CEC AB) loading onto AB

The effect of %Ag (w/w W_4O_{16}) added in $Ag_8W_4O_{16}$ photocatalyst impregnated into AB composite was shown in Figure 3. The optimal RhB removal efficiency was achieved with the 4%Ag@AB composite, reaching 66%, compared to 65% for pristine AB. Another phenomenon can be observed when the %removal of RhB increases from 2%Ag to 4%Ag, then decreases linearly as %Ag increases. This phenomenon can be caused by photocatalytic corrosion in which excess Ag^+ particles at higher Ag% concentration react with OH^- in water species, forming AgOH, which is stable (Thangavel et al., 2017), and Ag^+ particles can be further adsorbed onto composite surface (Huang et al., 2022) thus reducing overall photocatalytic efficiency in removing RhB. Figure 3 also shows the effect of BS12 surfactant concentration (%CEC AB) on the %removal of RhB. The optimum removal efficiency was achieved by 50%CEC@AB at 59%, which was lower than that of 4%Ag@AB and pristine AB, at 66% and 65%, respectively. The low removal of RhB of 50%CEC@AB can be attributed to the hydrophilic nature of the surfactant, which tends to lead to aggregation effects between composites, thereby lowering the adsorption capability, as shown by the SEM results (He et al., 2023).

Effect of pH

The effect of pH on the removal efficiency of RhB by AB, Ag@AB, and Ag@OAB composites and their corresponding pHpzc values is shown in Figure 4(a) and 4(b), respectively. For all composites, the RhB removal efficiency decreased with increasing pH from 4 to 12. All composites show the optimum removal efficiency at pH 4, with RhB removal rates of 67%, 71%, and 44% for AB, Ag@AB, and Ag@OAB, respectively. Figure 4 also shows the pHpzc values of AB, Ag@AB, and Ag@OAB, which are 4.6, 7.6, and 8.3, respectively. The point of zero charge (pHpzc) plays a crucial role in the adsorption-photocatalytic process, as changes in the RhB solution pH can influence the surface charge of the composites. When the pHpzc is lower than the solution pH, the composite surface becomes positively charged. Conversely, when the pHpzc is higher than the solution pH, the surface becomes negatively charged (Laysandra et al., 2018).

The pHpzc values of all three composites are higher than the optimum pH, indicating that their surfaces exhibit a positive charge at pH 4, which enhances electrostatic interactions with the zwitterionic form of the RhB dye (Rao et al., 2020). This phenomenon can be attributed to the chemical structure of RhB, which contains two distinct

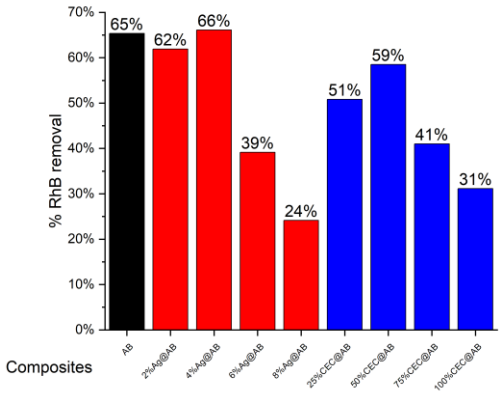

Figure 3. %Removal of RhB by Ag% and BS12 surfactant loading onto AB
(RhB: 50 mg/L, $m_{composite}$: 0.2 g, pH 6.5)

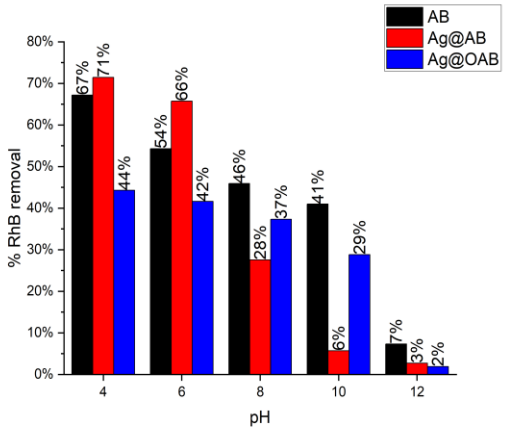

Figure 4(a). %Removal of RhB by pH
(RhB: 50 mg/L, $m_{composite}$: 0.2 g)

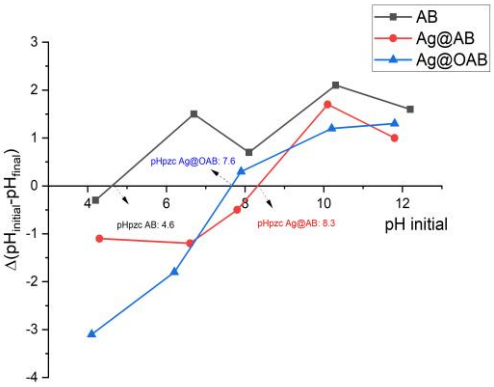

Figure 4(b). pHpzc of AB, Ag@AB, and Ag@OAB composites
($m_{composite}$: 0.2 g)

functional groups: the xanthene group (R = N^+–R) and the carboxyl group (R–COO^-), both of which can be protonated or deprotonated depending on the pH (Shrestha, 2021). At relatively low pH values, RhB can exist in different ionic forms: RhB^+ at pH 1.0–3.0, RhB^{2+} at pH <1.0, and RhB± (zwitterionic form) at pH >4.0 (Bhattacharyya et al., 2014). At pH 4, RhB primarily exists in its zwitterionic form, which is readily attracted to the positively charged surfaces of the three composites via electrostatic interaction. However, the xanthane group (R = N^+–R) in RhB may reduce the overall electrostatic attraction, slightly lowering the removal efficiency of RhB. As the pH increases, zwitterionic RhB tends to form aggregates due to electrostatic interactions between the xanthene and carboxyl groups with other RhB molecules (Bello et al., 2017). This aggregation increases the size of RhB molecules, in turn reduces the RhB removal efficiency at pH values higher than 4.

Removal of RhB Through Adsorption Photocatalytic Mechanism

The impregnation of $Ag_8W_4O_{16}$ photocatalyst and the intercalation of dodecyldimethylbetaine (BS12) into pristine AB resulted in distinct effects on RhB dye removal. The resulting composites (AB, Ag@AB and Ag@OAB) produced from all these materials showed two distinct removal mechanisms, which are adsorption for pristine AB, and adsorption–photocatalytic for Ag@AB and Ag@OAB composites. The AB composite showed adsorption mechanism of Rhodamine B (RhB) molecules onto the pristine montmorillonite surface, whereas addition of $Ag_8W_4O_{16}$ photocatalyst onto AB as Ag@AB composite promotes further degradation of RhB through synergistic adsorption-photocatalytic mechanism. However, the intercalation of zwitterionic BS12 surfactant in Ag@OAB composite alters the surface affinity of the material and further reduces RhB adsorption through electrostatic interaction, as RhB predominantly exists in a zwitterionic form under acidic conditions, particularly at pH 4.

The adsorption and photocatalytic reaction of RhB by the three composites can be expressed through equation (5) to (9) as follows:

$$AB^+ + RhB^{\pm} \xrightarrow{adsorption} AB \cdot RhB \quad (5)$$

$$Ag@AB^+ + RhB^{\pm} \xrightarrow{adsorption} Ag@AB \cdot RhB \quad (6)$$

$$Ag@AB + RhB \xrightarrow{photocatalytic} end\ product + CO_2 \quad (7)$$

$$Ag@OAB^+ + RhB^{\pm} \xrightarrow{adsorption} Ag@OAB \cdot RhB \quad (8)$$

$$Ag@OAB + RhB \xrightarrow{photocatalytic} end\ product + CO_2 \quad (9)$$

At pH 4, all composites exhibited positively charged surfaces, while RhB predominantly existed in its zwitterionic form. The superscripts (+) and (±) denote the surface charge of the composites and the ionic state of RhB, respectively.

Impregnation of $Ag_8W_4O_{16}$ photocatalyst in Ag@AB and Ag@OAB resulted in a distinct photocatalytic mechanism compared to pristine AB alone. However, the photocatalytic mechanism for this photocatalyst is not well understood. Therefore, analogous silver-tungstate metal-based photocatalysts such as $AgWO_3$ and Ag_2WO_4 were used to describe the mechanism. Same as other silver-tungstate photocatalyst, $Ag_8W_4O_{16}$ undergoes photoexitation under UV-visible light irradiation at λ = 400–700 nm. The tetratungstate (W_4O_{16}) absorbs photon energy from light source, which facilitates the transfer of electrons from the valence band (VB) to the conduction band (CB). Additionally. the presence of Ag nanoparticles in tetratungstate framework lowers the energy needed for electron transfer (Ramkumar & Rajarajan, 2016).

The photocatalytic degradation of RhB mediated by the $Ag_8W_4O_{16}$ photocatalyst can be represented by the following reactions (Matalkeh et al., 2022): The photocatalytic degradation of RhB by the $Ag_8W_4O_{16}$ photocatalyst can be summarized through equation (10) to (18) by the following reactions:

$$Ag@AB \xrightarrow{visible\ light} e^- + h^+ \quad (10)$$

$$Ag@OAB \xrightarrow{visible\ light} e^- + h^+ \quad (11)$$

$$h^+ + H_2O \rightarrow H^+ + OH^- \quad (12)$$

$$h^+ + OH^- \rightarrow OH^* \quad (13)$$

$$e^- + O_2 \rightarrow O_2^{*-} \quad (14)$$

$$O_2^{*-} + e^- \rightarrow 2H^+ + H_2O_2 \quad (15)$$

$$O_2^{*-} + H_2O_2 \rightarrow OH^* + OH^- + O_2 \quad (16)$$

$$O_2^{*-} + RhB \rightarrow end\ product + CO_2 \quad (17)$$

$$OH^* + RhB \rightarrow end\ product + CO_2 \quad (18)$$

The photocatalytic reactions above can be explained as follows: the degradation of RhB begins when the $Ag_8W_4O_{16}$ photocatalyst in Ag@AB (10) and Ag@OAB (11) absorbs light energy, promoting the transfer of electrons (e^-) from the valence band (VB) to the conduction band (CB), thereby leaving electron holes (h^+). This electron excitation within the Ag nanoparticles and tetratungstate structure results in the accumulation of electrons on the photocatalyst surface. The photogenerated electrons (12,13) subsequently react with molecular oxygen (O_2) to produce superoxide radicals (O_2•$^-$) and hydrogen peroxide (H_2O_2), while the corresponding photogenerated holes (14,15) oxidize water molecules (H_2O) to generate hydroxyl radicals (•OH). Both reactive oxygen species, O_2•$^-$ and •OH, drive the oxidative degradation of RhB (16,17,18), ultimately leading to the mineralization of the dye into harmless end-products, carbon dioxide (CO_2) and water.

Economic Feasibility: Composites Regeneration and Fabrication Cost

The regeneration performance and economic feasibility of AB, Ag@AB, and Ag@OAB composites were further investigated to determine the composites' potential for practical implementation. The

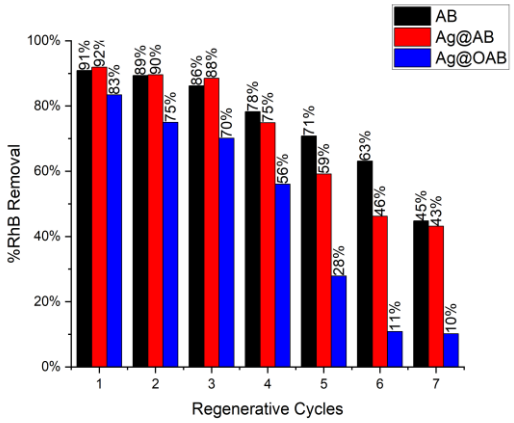

Figure 5. AB, Ag@AB and Ag@OAB composite Regeneration
(RhB: 200 mg/L, $m_{composite}$: 1 g, pH: 4, t: 60 min)

comparison between three composites may serve as a reference for evaluating the feasibility of applying the composite adsorbents (AB, Ag@AB, and Ag@OAB) in industrial settings (Cheng et al., 2020). Figure 5 illustrates the regeneration results of the AB, Ag@AB, and Ag@OAB composites. The results indicate that the AB composite exhibits a high regenerative capacity, maintaining a 70% removal of 70% in the fifth cycle. In comparison, Ag@AB maintains this efficiency up to the fourth cycle, while Ag@OAB, sustained it until the third cycle. The removal efficiency of all composites decreased progressively with successive regeneration cycles. This decline indicates a reduction in adsorption and photocatalytic performance due to the accumulation of RhB adsorbates on the composite structures during repeated desorption and washing processes (Ajel & Al-Nayili, 2023). Table 1 presents a comparison of the performance of various prepared bentonite composites in removing different adsorbates and their regenerative abilities. This comparison highlights the practical advantages of AB, Ag@AB, and Ag@OAB compared with other composites. The AB composite exhibited adsorption performance comparable to that of pristine MERCK bentonite. However, its regeneration capacity was slightly lower: the removal efficiency of methylene blue by pristine bentonite remained at 95% after the third cycle, whereas AB retained only 86%, as illustrated in Figure 5. The Ag@AB composite exhibited superior performance compared to other silver tungstate–bentonite composites and was comparable to pristine Ag_2WO_4 nanorods. Nevertheless, the pristine Ag_2WO_4 nanorods exhibited a faster removal rate, achieving complete methyl orange removal within 30 min, while Ag@AB required 90 min to remove RhB. The performance of the Ag@OAB composite was comparable to that of the CAPB@bentonite composite. Overall, the AB, Ag@AB and Ag@OAB composites demonstrated performance comparable to other similar reported composites.

The composite fabrication cost comparison may be used as a reference for evaluating the feasibility of applying the AB, Ag@AB, and Ag@OAB composites in industrial applications (Cheng et al., 2020). Table 2 presents the cost calculations required to produce 100 g of the AB, Ag@AB, and Ag@OAB composites, based on the total costs for raw material procurement and electricity consumption. All raw material costs are calculated excluding taxes, and electricity costs are estimated based on the Indonesian 2025 Electricity Tariff for the P-3/TR (Electricity Tariff for Government Agencies) category,

Tabel 1. Reported Results on Various Composites in terms of Adsorbate Removal and Regeneration Abilities

Preparation method	Composites	Adsorbate	%Removal	Regeneration abilities	Ref.
Without any purification	Natural bentonite	Methylene blue	99.5% (60 min)	-	(Jawad et al., 2023)
H_2SO_4 pretreatment	Activated bentonite	Congo red	80% (30 min)	-	(Taher et al., 2019)
MERCK procurement	Pristine bentonite	Methylene blue	95% (60 min)	95% (3^{rd} cycles)	(Farhan binti Azha et al., 2021)
HCl pretreatment	**Activated bentonite (AB)**	**Rhodamine B**	**91% (60 min)**	**71% (5^{th} cycles)**	**Present work**
Co-precipitation	Pristine Ag_2WO_4 nanorods	Methyl orange	90% (30 min)	80% (4^{th} cycles)	(Andrade Neto et al., 2019)
Dry impregnation	$AgWO_3$-AB	Humic acid	80% (180 min)	75% (5^{th} cycles)	(Ajel & Al-nayili, 2023)
Wet impregnation	$Ag@Ag_8W_4O_{16}$-nanoroasted rice	Rhodamine B	80% (50 min)	-	(Selvamani et al., 2016)
Wet impregnation	**Ag@AB**	**Rhodamine B**	**92% (60 min)**	**75% (4^{th} cycles)**	**Present work**
Simple mixing	BS12-Bentonite	Pb^{2+} ions	70% (60 min)	-	(He et al., 2023)
Simple mixing	CAPB@bentonie	Reactive Yellow 160	80% (60 min)	-	(Abdel Ghafar et al., 2020)
Simple mixing	HDTA-bentonite	Tannin	99.6% (360 min)	90.2% (4^{th} cycles)	(Anirudhan & Ramachandran, 2006)
Simple mixing	**Ag@OAB**	**Rhodamine B**	**83% (60 min)**	**70% (3^{rd} cycles)**	**Present work**

Table 2. Total Fabrication Cost for Producing 100 g of AB, Ag@AB, and Ag@OAB composites

Raw Material	Ratio (g)	Cost (IDR/g)	Material cost for 100 g AB (IDR)	Material cost for 100 g Ag@AB (IDR)	Material cost for 100 g Ag@OAB (IDR)
Natural bentonite	80	0	0	0	0
$Na_2WO_4 .2H_2O$	28.56	271,320	0	271,320	271,320
$AgNO_2$	1.27	31,750	0	31,750	31,750
BS12	483.6	30,950	0	0	30,950
HCl	39.33	6,293	6,293	6,293	6,293
Citrate	1.2	5,100	0	5,100	5,100
Total Raw Material Cost (IDR)			6,293	314,463	345,413
Total Raw Material Cost (US$)			0.38	18.87	20.72
The Fabrication Cost for 100 g of Composite					
Equipment	**Power (kW)**	**Electrical Tariff (IDR/kWh)**	**Duration of usage (h)**		
			AB	**Ag@AB**	**Ag@OAB**
Oven	1	1444.7	12	24	36
Hotplate	0.6		1	3	4
Total Electricity (kWh)			12.6	25.8	38.4
Production Cost (IDR)			18,203	37,273	554,76
TFC = Raw Material Cost + Production Cost (IDR)			24,496	351,736	400,890
TFC (US$)			**1.47**	**21.10**	**24.05**

which is Rp 1,444.70/kWh (PT PLN (Persero), 2025). The total production costs for Ag@AB and Ag@OAB are 14 and 16 times higher, respectively, compared to those of AB alone.

CONCLUSION

The AB, Ag@AB, and Ag@OAB composites were successfully synthesized. Acid-activated bentonite (AB) was prepared using HCl pretreatment of natural bentonite, followed by wet impregnation with $Ag_8W_4O_{16}$ photocatalyst to produce Ag@AB. Subsequently, Ag@OAB was synthesized by intercalating the BS12 surfactant into the Ag@AB composite. Scanning electron microscopy (SEM) was employed to characterize the surface morphologies of the composites. Variations in Ag loading (% w/w W_4O_{16}) and BS12 concentration on AB significantly affected RhB removal. The 4% Ag@AB composite achieved the highest removal efficiency (66%), slightly higher than that of pristine AB (65%). In contrast, the 50% CEC@AB composite reached only 59%, indicating reduced performance compared with 4% Ag@AB and pristine AB.The pH of 4 was found to be the optimum pH for removing RhB. The maximum removal percentage was achieved at pH 4 for the AB, Ag@AB, and Ag@OAB composites with RhB removal percentages of 67%, 71%, and 44%, respectively. The increase in removal percentages was attributed to changes in the surface charge of the composites. The pHpzc of AB, Ag@AB, and Ag@OAB composites were 4.6, 7.6, and 8.3, respectively, which are lower than the optimum pH, indicating positive surface charge on all three composites. Although a positive surface charge enhances the removal of RhB due to electrostatic attraction, electrostatic repulsion between the positive surface charge of the composite, and the zwitterionic group of RhB may lower the removal efficiency of RhB.

According to the regeneration performance study, the AB composite retained 70% of its RhB removal efficiency after the fifth cycle, whereas Ag@AB and Ag@OAB maintained their performance only up to the fourth and third cycles, respectively. The fabrication cost for the AB composite is 14 to 16 times cheaper than that for Ag@AB and Ag@OAB, respectively. In summary, the impregnation of the $Ag_8W_4O_{16}$ photocatalyst onto AB, resulting in the Ag@AB composite, increases the overall RhB removal efficiency compared to pristine AB. In contrast, the intercalation of the BS12 surfactant in Ag@OAB composite led to a decrease in removal performance, yielding the lowest RhB removal efficiency among the three composites.

CONFLICT OF INTEREST

The authors declare that they have no known competing financial interests or personal relationships that could have appeared to influence the work reported in this paper.

ACKNOWLEGMENTS

The authors would like to thank the Department of Chemical Engineering for its support and facilities provided for this research.

NOTATION

Symbol	Definition	Unit
AB	Acid-activated bentonite composite	-
Ag@AB	$Ag_8W_4O_{16}$ photocatalyst-loaded AB composite.	-

Ag@OAB	BS12 surfactant-intercalated Ag@AB composite	-
BS12	Dodecyl dimethyl betaine	-
CEC	Cation exchange capacity	meq/ 100 g
RhB	Rhodamine B	-
pHpzc	pH points of zero charge	-
%Removal	Percentage of RhB removal	%
SEM	Scanning Electron Microscopy	-
%w/w	Weight per weight	%

REFERENCES

Abdel Ghafar, H. H., Radwan, E. K., & El-Wakeel, S. T. (2020). Removal of Hazardous Contaminants from Water by Natural and Zwitterionic Surfactant-modified Clay. *ACS Omega*, *5*(12), 6834–6845. https://doi.org/10.1021/acsomega.0c00166

Ajel, M. K., & Al-nayili, A. (2023). Synthesis, characterization of Ag-WO3/bentonite nanocomposites and their application in photocatalytic degradation of humic acid in water. *Environmental Science and Pollution Research*, *30*(8), 20775–20789. https://doi.org/10.1007/s11356-022-23614-4

Andrade Neto, N. F., Oliveira, P. M., Bomio, M. R. D., & Motta, F. V. (2019). Effect of temperature on the morphology and optical properties of Ag2WO4 obtained by the co-precipitation method: Photocatalytic activity. *Ceramics International*, *45*(12), 15205–15212. https://doi.org/10.1016/j.ceramint.2019.05.006

Anirudhan, T. S., & Ramachandran, M. (2006). Adsorptive removal of tannin from aqueous solutions by cationic surfactant-modified bentonite clay. *Journal of Colloid and Interface Science*, *299*(1), 116–124. https://doi.org/10.1016/j.jcis.2006.01.056

Aslam, M., Soomro, M. T., Ismail, I. M. I., Salah, N., Ashraf, M. W., Qari, H. A., & Hameed, A. (2019). The performance of silver modified tungsten oxide for the removal of 2-CP and 2-NP in sunlight exposure: Optical, electrochemical and photocatalytic properties. *Arabian Journal of Chemistry*, *12*(8), 2632–2643. https://doi.org/10.1016/j.arabjc.2015.05.001

Balakrishnan, A., Gopalram, K., & Appunni, S. (2021). Photocatalytic degradation of 2,4-dicholorophenoxyacetic acid by TiO2 modified catalyst: Kinetics and operating cost analysis. *Environmental Science and Pollution Research*, *28*(25), 33331–33343. https://doi.org/10.1007/s11356-021-12928-4

Bello, O. S., Lasisi, B. M., Adigun, O. J., & and, V. E. (2017). Scavenging Rhodamine B dye using moringa oleifera seed pod. *Chemical Speciation & Bioavailability*, *29*(1), 120–134. https://doi.org/10.1080/09542299.2017.1356694

Bhattacharyya, K. G., SenGupta, S., & Sarma, G. K. (2014). Interactions of the dye, Rhodamine B with kaolinite and montmorillonite in water. *Applied Clay Science*, *99*, 7–17. https://doi.org/10.1016/j.clay.2014.07.012

Chandanshive, V. V., Kadam, S. K., Khandare, R. V., Kurade, M. B., Jeon, B.-H., Jadhav, J. P., & Govindwar, S. P. (2018). In situ phytoremediation of dyes from textile wastewater using garden ornamental plants, effect on soil quality and plant growth. *Chemosphere*, *210*, 968–976. https://doi.org/10.1016/j.chemosphere.2018.07.064

Cheng, D., Ngo, H. H., Guo, W., Chang, S. W., Nguyen, D. D., Zhang, X., Varjani, S., & Liu, Y. (2020). Feasibility study on a new pomelo peel derived biochar for tetracycline antibiotics removal in swine wastewater. *Science of The Total Environment*, *720*, 137662. https://doi.org/10.1016/j.scitotenv.2020.137662

Djebri, N., Boutahala, M., Chelali, N. E., Boukhalfa, N., & Zeroual, L. (2016). Enhanced removal of cationic dye by calcium alginate/organobentonite beads: Modeling, kinetics, equilibriums, thermodynamic and reusability studies. *International Journal of Biological Macromolecules*, *92*, 1277–1287. https://doi.org/10.1016/j.ijbiomac.2016.08.013

Farhan binti Azha, S., Woon, L., & Ismail, S. (2021). Regeneration Feasibility of Bentonite by Sodium Persulfate. *Trends Journal of Sciences Research*, *10.31586*, 1–10. https://doi.org/10.31586/wastewater101002

He, Y., Wen, M., Xu, B., Tang, Q., Xiao, J., He, B., Xu, J., Shen, W., & Gou, S. (2023). Flexible structural regulation of montmorillonite through intercalation by zwitterionic surfactants for effective removal of methylene blue. *Journal of Molecular Liquids*, *391*, 123349. https://doi.org/10.1016/j.molliq.2023.123349

Huang, K., Li, C., Zheng, Y., Wang, L., Wang, W., & Meng, X. (2022). Recent advances on silver-based photocatalysis: Photocorrosion inhibition, visible-light responsivity enhancement, and charges separation acceleration. *Separation and Purification Technology*, *283*, 120194. https://doi.org/10.1016/j.seppur.2021.120194

Hussain, B., Yaseen, H., Khalid-Al-Ghanim, Al-Misned, F., Qasim, M., Al-Mulhm, N., & Mahboob, S. (2021). A study on risk assessment of effect of hematoxylin dye on cytotoxicity and nephrotoxicity in

freshwater fish: Food and water security prospective research. *Saudi Journal of Biological Sciences*, *28*(4), 2267–2271. https://doi.org/10.1016/j.sjbs.2021.01.019

Islam, T., Repon, Md. R., Islam, T., Sarwar, Z., & Rahman, M. M. (2023). Impact of textile dyes on health and ecosystem: A review of structure, causes, and potential solutions. *Environmental Science and Pollution Research*, *30*(4), 9207–9242. https://doi.org/10.1007/s11356-022-24398-3

Jawad, A. H., Saber, S. E. M., Abdulhameed, A. S., Farhan, A. M., ALOthman, Z. A., & Wilson, L. D. (2023). Characterization and applicability of the natural Iraqi bentonite clay for toxic cationic dye removal: Adsorption kinetic and isotherm study. *Journal of King Saud University - Science*, *35*(4), 102630. https://doi.org/10.1016/j.jksus.2023.102630

Laysandra, L., Santosa, F. H., Austen, V., Soetaredjo, F. E., Foe, K., Putro, J. N., Ju, Y. H., & Ismadji, S. (2018). Rarasaponin-bentonite-activated biochar from durian shells composite for removal of crystal violet and Cr(VI) from aqueous solution. *Environmental Science and Pollution Research*, *25*(30), 30680–30695. https://doi.org/10.1007/s11356-018-3104-x

Laysandra, L., Sari, M. W. M. K., Soetaredjo, F. E., Foe, K., Putro, J. N., Kurniawan, A., Ju, Y.-H., & Ismadji, S. (2017). Adsorption and photocatalytic performance of bentonite-titanium dioxide composites for methylene blue and rhodamine B decoloration. *Heliyon*, *3*(12), e00488. https://doi.org/10.1016/j.heliyon.2017.e00488

Li, Y., Yang, D., Cheng, F., Li, Z., & Wu, D. (2023). Regulating interlayer and surface properties of montmorillonite by dodecyl dimethyl betaine for enhanced lead ion capture. *Surfaces and Interfaces*, *42*, 103348. https://doi.org/10.1016/j.surfin.2023.103348

Markandeya, Mohan, D., & Shukla, S. P. (2022). Hazardous consequences of textile mill effluents on soil and their remediation approaches. *Cleaner Engineering and Technology*, *7*, 100434. https://doi.org/10.1016/j.clet.2022.100434

Matalkeh, M., Nasrallah, G. K., Shurrab, F. M., Al-Absi, E. S., Mohammed, W., Elzatahry, A., & Saoud, K. M. (2022). Visible Light Photocatalytic Activity of Ag/WO3 Nanoparticles and its Antibacterial Activity Under Ambient Light and in The Dark. *Results in Engineering*, *13*, 100313. https://doi.org/10.1016/j.rineng.2021.100313

Nan, J., Liu, X., Zhang, D., Xu, R., & Zhang, Y. (2025). Application of Porous Materials in Photocatalytic Treatment of Wastewater. *Colloids and Interfaces*, *9*(1). https://doi.org/10.3390/colloids9010003

PT PLN (Persero). (2025). *Penetapan Penyesuaian Tarif Tenaga Listrik (Tariff Adjustment) April—Juni 2025*. PT PLN (Persero). https://web.pln.co.id/pelanggan/tarif-tenaga-listrik/tariff-adjustment

Rafiq, A., Ikram, M., Ali, S., Niaz, F., Khan, M., Khan, Q., & Maqbool, M. (2021). Photocatalytic degradation of dyes using semiconductor photocatalysts to clean industrial water pollution. *Journal of Industrial and Engineering Chemistry*, *97*, 111–128. https://doi.org/10.1016/j.jiec.2021.02.017

Ramadhan, A., Fathurrohman, M. I., & Soegijono, B. (2015). Chemical Modification of Upgraded Bentonite as Filler of Natural Rubber/Organobentonite Composite. *Procedia Chemistry*, *16*, 85–90. https://doi.org/10.1016/j.proche.2015.12.028

Ramkumar, S., & Rajarajan, G. (2016). Enhanced visible light photocatalytic activity of pristine and silver (Ag) doped WO3 nanostructured thin films. *Journal of Materials Science: Materials in Electronics*, *27*(11), 12185–12192. https://doi.org/10.1007/s10854-016-5373-9

Rao, W., Piliouras, P., Wang, X., Guido, A., Kugler, K., Sieren, B., Wang, L., Lv, G., & Li, Z. (2020). Zwitterionic dye rhodamine B (RhB) uptake on different types of clay minerals. *Applied Clay Science*, *197*, 105790. https://doi.org/10.1016/j.clay.2020.105790

Ren, S., Deng, J., Meng, Z., Wang, T., Xie, T., & Xu, S. (2019). Enhanced removal of phenol by novel magnetic bentonite composites modified with amphoteric-cationic surfactants. *Powder Technology*, *356*, 284–294. https://doi.org/10.1016/j.powtec.2019.08.024

Rihayat, T., Salim, S., Arlina, A., Fona, Z., Jalal, R., Alam, P., Zaimahwati, Z., Sami, M., Syarif, J., & Juhan, N. (2018). Determination of CEC value (Cation Exchange Capacity) of Bentonites from North Aceh and Bener Meriah, Aceh Province, Indonesia using three methods. *IOP Conference Series: Materials Science and Engineering*, *334*, 012054. https://doi.org/10.1088/1757-899X/334/1/012054

Saha, N., Volpe, M., Fiori, L., Volpe, R., Messineo, A., & Reza, M. T. (2020). Cationic Dye Adsorption on Hydrochars of Winery and Citrus Juice Industries Residues: Performance, Mechanism, and Thermodynamics. *Energies*, *13*, 4686. https://doi.org/10.3390/en13184686

Selvamani, M., Krishnamoorthy, G., Ramadoss, M., Sivakumar, P. K., Settu, M., Ranganathan, S., & Vengidusamy, N. (2016). Ag@Ag8W4O16 nanoroasted rice beads with photocatalytic, antibacterial and anticancer activity. *Materials Science and Engineering: C*, *60*, 109–118. https://doi.org/10.1016/j.msec.2015.11.002

Shrestha, D. (2021). Efficiency of Wood-Dust of Dalbergia sisoo as Low-Cost Adsorbent for

Rhodamine-B Dye Removal. *Nanomaterials*, *11*(9). https://doi.org/10.3390/nano11092217

Taher, T., Rohendi, D., Mohadi, R., & Lesbani, A. (2019). Congo red dye removal from aqueous solution by acid-activated bentonite from sarolangun: Kinetic, equilibrium, and thermodynamic studies. *Arab Journal of Basic and Applied Sciences*, *26*(1), 125–136. https://doi.org/10.1080/25765299.2019.1576274

Thangavel, S., Thangavel, S., Raghavan, N., Alagu, R., & Venugopal, G. (2017). Efficient visible-light photocatalytic and enhanced photocorrosion inhibition of Ag2WO4 decorated MoS2 nanosheets. *Journal of Physics and Chemistry of Solids*, *110*, 266–273. https://doi.org/10.1016/j.jpcs.2017.06.005

Ulhaq, I., Ahmad, W., Ahmad, I., Yaseen, M., & Ilyas, M. (2021). Engineering TiO2 supported CTAB modified bentonite for treatment of refinery wastewater through simultaneous photocatalytic oxidation and adsorption. *Journal of Water Process Engineering*, *43*, 102239. https://doi.org/10.1016/j.jwpe.2021.102239

Wang, X., Li, S., Yu, H., & Yu, J. (2011). In situ anion-exchange synthesis and photocatalytic activity of Ag8W4O16/AgCl-nanoparticle core–shell nanorods. *Journal of Molecular Catalysis A: Chemical*, *334*(1), 52–59. https://doi.org/10.1016/j.molcata.2010.10.022

Wang, X., Zhan, S., Wang, Y., Wang, P., Yu, H., Yu, J., & Hu, C. (2014). Facile synthesis and enhanced visible-light photocatalytic activity of Ag2S nanocrystal-sensitized Ag8W4O16 nanorods. *Journal of Colloid and Interface Science*, *422*, 30–37. https://doi.org/10.1016/j.jcis.2014.02.009

Warsono, H. R. S., Kurniawan, W., & Hinode, H. (2018). Utilization of modified indonesia natural bentonite for dye removal. *ASEAN Journal of Chemical Engineering*, *18*(2), 13–21. https://doi.org/10.22146/ajche.49532

Yang, S., Huang, Z., Li, C., Li, W., Yang, L., & Wu, P. (2020). Individual and simultaneous adsorption of tetracycline and cadmium by dodecyl dimethyl betaine modified vermiculite. *Colloids and Surfaces A: Physicochemical and Engineering Aspects*, *602*, 125171. https://doi.org/10.1016/j.colsurfa.2020.125171

Zinatloo-Ajabshir, S., Baladi, M., Amiri, O., & Salavati-Niasari, M. (2020). Sonochemical synthesis and characterization of silver tungstate nanostructures as visible-light-driven photocatalyst for waste-water treatment. *Separation and Purification Technology*, *248*, 117062. https://doi.org/10.1016/j.seppur.2020.117062